Journal of
Applied Crystallography
ISSN 0021-8898

Received 16 August 2006
Accepted 29 January 2007

Melting behavior of polymorphic crystals of poly(trimethylene 2,6-naphthalate) studied by simultaneous synchrotron X-ray scattering and thermal analysis

Wei-Tsung Chuang,[a] Po-Da Hong,[b]* Chih-Hua Chen,[b] Hwo-Shuenn Sheu[a] and U-Ser Jeng[a]

[a]National Synchrotron Radiation Research Center, Hsinchu 300, Taiwan, and [b]Department of Polymer Engineering, National Taiwan University of Science and Technology, Taipei 106, Taiwan. Correspondence e-mail: poda@mail.ntust.edu.tw

The polymorphic crystallization and melting behavior of poly(trimethylene 2,6-naphthalate) (PTN) have been investigated using small-angle X-ray scattering and simultaneous wide-angle X-ray scattering (WAXS) and differential scanning calorimetry (DSC). The α-crystal, the β-crystal and the coexistence of both crystal forms of PTN develop at an isothermal temperature below 393 K, above 453 K and between these two temperatures, respectively. The simultaneous WAXS/DSC measurement provides a good way to identify the origin of multiple melting peaks and to get equilibrium melting temperatures. During the PTN melting process, the thermal evolutions of crystallinities, Bragg diffraction intensities and DSC thermograms reveal that the $\alpha \rightarrow \beta$ phase transformation and primary and secondary crystallizations arise to generate the multiple melting peaks. The β-crystal with high equilibrium melting temperature ($T^0_{m,\beta}$ = 510 K) is a structurally stable phase while the α-crystal with low equilibrium melting temperature ($T^0_{m,\alpha}$ = 488 K) is a metastable phase. The temperature-dependent structural parameters such as the long period, lamellar thickness and amorphous thickness were extracted from the interface distribution function. Two-step changes in the lamellar thickness and the invariant during the subsequent melting of PTN crystallized at 383 K are consistent with the $\alpha \rightarrow \beta$ transformation obtained by WAXS/DSC. The $\alpha \rightarrow \beta$ transformation, a typical melting–recrystallization, proceeds firstly *via* surface melting of α-lamellae, and then the PTN chains near the boundaries of surviving α-lamellae modify their conformation to form the β-crystal resulting in thickening lamellae.

© 2007 International Union of Crystallography
Printed in Singapore – all rights reserved

1. Introduction

Poly(trimethylene 2,6-naphthalate) (PTN) is a semicrystalline polymer with a glass temperature of *ca* 353 K and a melting temperature of *ca* 483 K. For engineering plastic and textile fiber, the promising material of PTN with three methylene groups is like well known poly(trimethylene terephthalate) PTT. Numerous studies have been carried out on the crystallization and melting behaviors of PTT (Chuang *et al.*, 2002; Hong *et al.*, 2002). However, PTN has not received the attention it deserves yet. So far, only a few systematical studies have been carried out to investigate the melting behavior and polymorphic structure with the α-crystal (monoclinic) and β-crystal (triclinic) in PTN (Jeong *et al.*, 2003, 2004). A poor understanding of the relationship between polymorphic crystallization and melting behaviors hinders us in clarifying the processes.

Multiple melting peaks in a differential scanning calorimetry (DSC) thermogram carry a usual phenomenon of polymer crystallization, especially for the aromatic polyesters. The multiple melting behavior is usually explained by polydisperse lamellar thickness (dual lamellar thickness) (Cheng *et al.*, 1986; Hsiao *et al.*, 1993*a*, *b*), melting–recrystallization–remelting (Blundell & Osborn, 1983; Blundell, 1987) and polymorphic crystals (Sun & Woo, 1999; Ho *et al.*, 2000; Gan *et al.*, 2004; Ghosh *et al.*, 2005). Both the dual lamellar thickness and melting–recrystallization–remelting can easily be confirmed by DSC measurements at different scan rates and different annealing treatments (time and/or temperature). However, in the case of polymorphic PTN crystallization, the factors as above-mentioned possibilities make it difficult for us to identify the multiple melting when only relying on a calorimetric study.

We specifically utilize small-angle X-ray scattering (SAXS) and simultaneous wide-angle X-ray scattering and differential scanning calorimetry (WAXS/DSC) measurements to probe the multiple melting behavior and polymorphic crystallization in a PTN system. The goals of this study are: (i) to provide *in-situ* WAXS and DSC measurements to explain the observed polymorphic crystallization and melting behavior, (ii) to assign the multiple melting peaks to the corresponding polymorphism or primary/secondary crystallization, and (iii) to investigate the mechanism of the $\alpha \rightarrow \beta$ phase transformation.

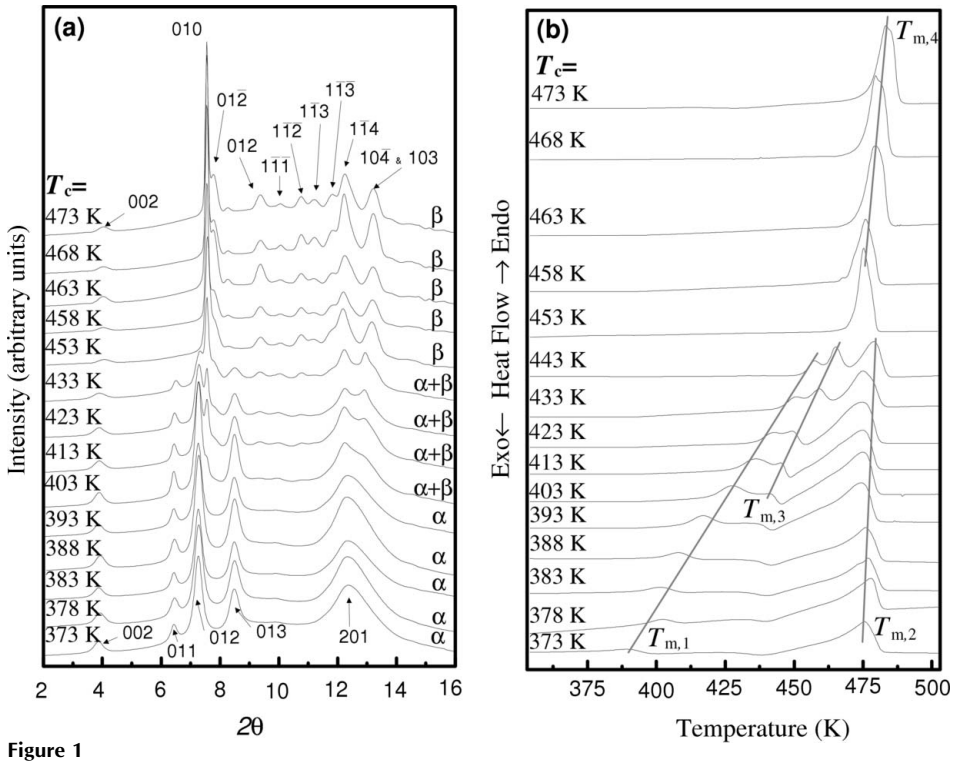

Figure 1
(*a*) WAXS profiles of PTN crystallized isothermally at various T_c. (*b*) DSC melting curves of polymorphic PTN after being crystallized at various T_c.

2. Experimental

2.1. Samples

Poly(trimethylene 2,6-naphthalate) (PTN), kindly supplied by Shell Chemical Company, has an intrinsic viscosity [η] of 0.6 dm^3 kg^{-1} measured in a mixed solvent of phenol/tetrachloroethane (6/4, *w*/*w*) at 298 K. For isothermal crystallization treatments, the samples were first melted at 553 K for 10 min in an oven and then transferred quickly (within a few seconds) into another oven at a desired isothermal temperature (T_c) to start crystallization for 24 h until complete crystallization.

2.2. Measurements

We used a Perkin–Elmer Pyris 1 DSC instrument equipped with a mechanical intracooler under nitrogen purge for observing melting curves. Another DSC instrument (Mettler–Toletro FP84) was combined with synchrotron X-ray scattering. For X-ray measurement, the samples were sealed inside DSC aluminium cells modified with two Kapton windows.

Synchrotron X-ray measurements were performed at beamlines BL01C (powder X-ray scattering endstation) and BL17B3 (a small-angle X-ray scattering endstation) of the National Synchrotron Radiation Research Center, Taiwan. The simultaneous WAXS/DSC measurement was performed at a wavelength λ = 0.775 Å. The WAXS data were collected on a MAR345 imaging plate detector. The scattering angle was calibrated from a mixture of silver behenate and silicon powders. The relative crystallinity derived from WAXS is defined as the ratio of the integrated intensity of all Bragg peaks observed to the integrated intensity of the whole WAXS profile of the PTN samples studied.

Small-angle X-ray scattering (SAXS) measurement was performed with X-ray wavelength λ = 1.9061 Å, using an area detector with a sample-to-detector distance of 1726 mm. The SAXS data were corrected for sample transmission, background and the detector sensitivity. The modulus of the scattering vector q [= $4\pi\sin(\theta/2)/\lambda$], defined by scattering angle θ and the wavelength λ of the X-rays, was calibrated by a standard sample of silver behenate. One-dimensional intensity profiles $I(q)$ were obtained from a circular integration of the two-dimensional isotropic scattering patterns of SAXS for better data statistics. The detailed SAXS setup and instrument calibration was reported on previously study (Lai *et al.*, 2006).

3. Results and discussion

3.1. Characterization of polymorphic PTN crystals

Fig. 1(*a*) shows the WAXS profiles of PTN crystallized at various isothermal temperatures (T_c) for 24 h. When T_c is lower than 393 K, only the α-crystal develops. As T_c increases above 403 K, however, both the α- and β-crystals coexist. When T_c is above 453 K, only the β-crystal remains stable. Fig. 1(*b*) shows the DSC thermograms (heating rate of 10 K min^{-1}) of the PTN samples, which were the same with as those in Fig. 1(*a*). Four melting peaks, labeled as $T_{m,1}$, $T_{m,2}$, $T_{m,3}$ and $T_{m,4}$, can be observed in the melting curves of PTN crystallized at various T_c. These melting peaks, except $T_{m,2}$, shift to higher temperatures as shown by the guide lines in Fig. 1(*b*) when T_c is increased. The broad exothermic peak (recrystallization peak) is visible around 443–463 K depending on the crystallization temperature for the samples crystallized at T_c = 373–443 K. Comparing WAXS profiles in Fig. 1(*a*) with DSC curves in Fig. 1(*b*), the melting behaviors of PTN can be classified into three types: (1) PTN crystallized at $T_c > 453$ K has only one melting endotherm, $T_{m,4}$; (2) PTN crystallized at $393 < T_c < 453$ K has three melting endotherms, $T_{m,1}$, $T_{m,2}$ and $T_{m,3}$; (3) PTN crystallized at $T_c < 393$ K has two melting endotherms, $T_{m,1}$ and $T_{m,2}$.

3.2. Identification of multiple melting peaks

To identify the origin of multiple melting peaks, simultaneous WAXS/DSC was used. Fig. 2(*a*) shows thermal evolution of WAXS profiles recorded during the melting process of the PTN α-crystal prepared at 383 K for 24 h. Except for the Bragg peaks of the α-crystal, three obvious Bragg peaks of the β-crystal [$1\bar{1}\bar{1}_\beta$, $1\bar{1}4_\beta$ and $10\bar{4}_\beta$ as marked by the arrows in Fig. 2(*a*)] take place after the sample heated to 443 K, indicating that the partial α-crystal may be transformed into the β-crystal during the heating process. It must be noted, however, that the WAXS profile measured during the $\alpha \rightarrow \beta$ transformation is different from that of the coexistence of α- and β-crystals [see Fig. 1(*a*)]. This means that the crystallization structure formed in the $\alpha \rightarrow \beta$ transformation is different from that of the coexistence phases. Fig. 2(*b*) summarizes the DSC thermogram, normalized crystallinity and WAXS intensities of emblematic diffraction peaks for both α- and β-crystals from WAXS/DSC measurements at the heating rate of 3 K min^{-1}. The normalized crystallinities are defined as the relative crystallinities at various temperatures being normalized by that measured at T_c. When the temperature is raised to $T_{m,1}$

(~398 K), the Bragg peaks of the α-crystal still exist and the total normalized crystallinity $W_{c,total}$ decreases *ca* 4%, implying that $T_{m,1}$ can not absolutely be referred to as the major melting temperature of the α-crystal.

In Fig. 1(*b*), the low endotherm $T_{m,1}$ obtained at ~10 K above T_c is usually attributed to an annealing effect (Cheng *et al.*, 1986; Velikov & Marand, 1993). We also found that the low endotherm $T_{m,1}$ not only shifts to a higher temperature with increase of the crystallization temperature, but also increases in magnitude with the annealing time. For typical polymer crystallization, thicker lamellar stacks usually develop first in the primary crystallization, and then thinner lamellar stacks or imperfect crystals grow within the remnant spacing in the secondary crystallization. The melting behaviors of thinner and thicker lamellae can be associated with the low and high endothermic peaks, respectively. We attribute the low endotherm of $T_{m,1}$ to the melting of the secondary α-crystal. Only the decrease of 4% in $W_{c,total}$ through $T_{m,1}$ [see Fig. 2(*b*)] manifests that the secondary α-crystal formed at T_c = 383 K is of a lower quality than the primary α-crystal, even though it may form a mesophase at most.

For the $\alpha \rightarrow \beta$ transformation during the melting process, the total normalized crystallinity $W_{c,total}$ can be separated into two crystallinities of $W_{c,\alpha}$ (α-crystal) and $W_{c,\beta}$ (β-crystal) by the deconvolution of WAXS profiles. The crystallinity $W_{c,\alpha}$ and Bragg diffraction intensities of the α-crystal (011_α, 012_α and 201_α) significantly decrease at ~466 K, whereas, the crystallinity $W_{c,\beta}$ and intensities of the β-crystal ($1\bar{1}4_\beta$ and $10\bar{4}_\beta$) exhibit a maximum value at ~473 K. In Fig. 2(*b*), the Bragg peaks of the β-crystal appear to be accompanied by the broad exothermic peak at ~443 K. Due to the peak of $T_{m,2}$ broadening at the low temperature side as indicated by overlapped melting peaks, we can reasonably deconvolute $T_{m,2}$ into two melting peaks of $T_{m,2}'$ and $T_{m,2}''$. To compare the DSC thermogram with the changes in $W_{c,\alpha}$ and $W_{c,\beta}$, we use the onset temperatures of $W_{c,\alpha}$ and $W_{c,\beta}$ deviated from the baseline to define, respectively, the melting peaks of $T_{m,2}'$ and $T_{m,2}''$ as the arrows shown in Fig. 2(*b*). The melting of the primary α-crystal gives $T_{m,2}'$ and the melting of the β-crystal transformed from the α-crystal gives $T_{m,2}''$. From the variations of $W_{c,\alpha}$ and $W_{c,\beta}$, the recrystallization of the β-crystal, however, cannot

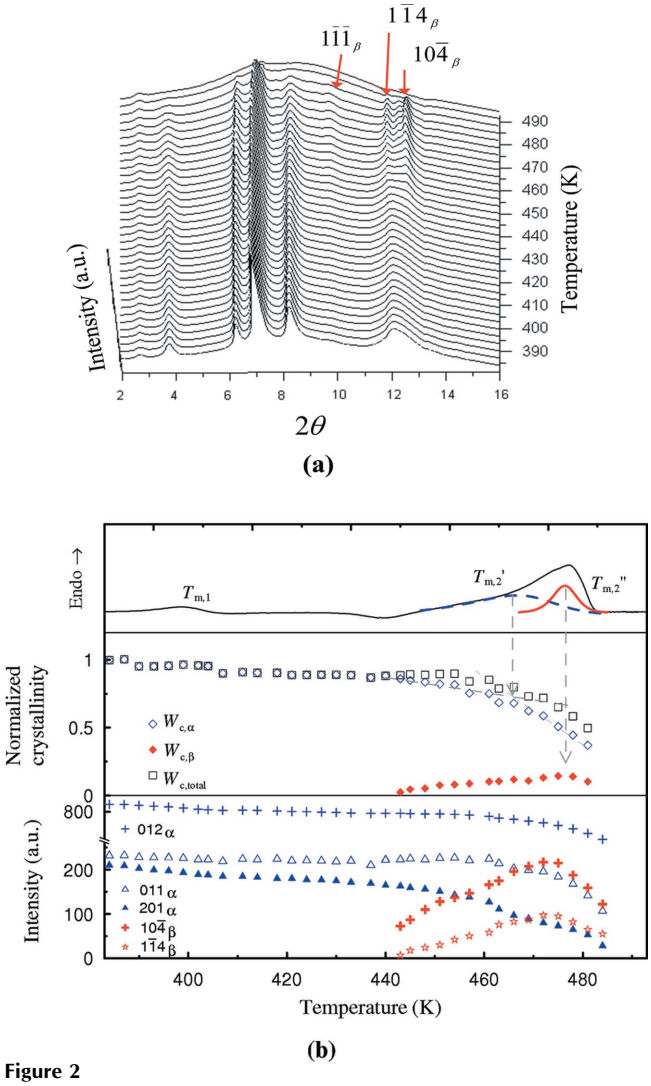

Figure 2
(*a*) Temperature scan of WAXS profiles recorded during the melting process (3 K min^{-1}) of PTN crystallized at T_c = 383 K. Three Bragg peaks of the β-crystal are marked by arrows. (*b*) Thermal evolution of structural characterization during the melting process (3 K min^{-1}) of PTN crystallized at T_c = 383 K: DSC thermogram (top), normalized crystallinity (middle) and intensity of Bragg diffraction peaks (bottom).

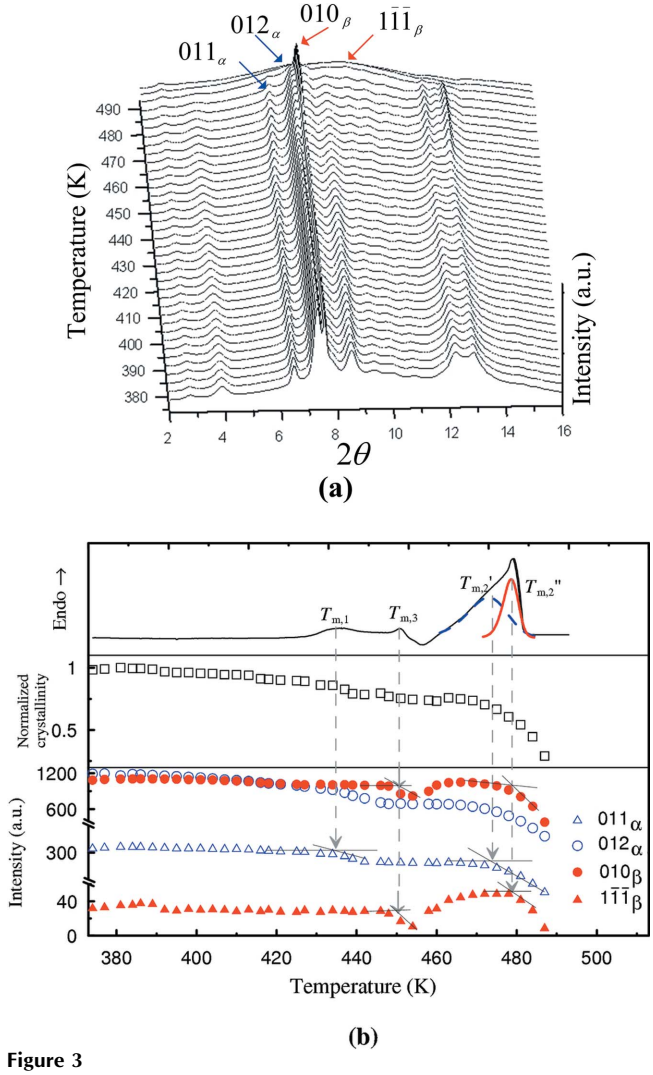

Figure 3
(*a*) Temperature scan of WAXS profiles recorded during the melting process (3 K min^{-1}) of PTN crystallized at T_c = 423 K. (*b*) Thermal evolution of structural characterization during the melting process of the PTN coexistent form of α- and β-crystals: DSC thermogram (top), normalized crystallinity (middle) and intensity of Bragg diffraction peaks (bottom). The solid circle and triangle are Bragg peaks of the β-crystal and the open circle and triangle are Bragg peaks of the α-crystal. Those emblematic peaks are marked by (*a*).

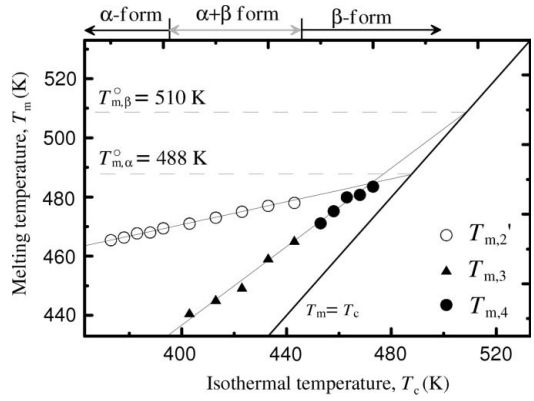

Figure 4
Hoffman–Weeks extrapolation for polymorphic crystals of PTN.

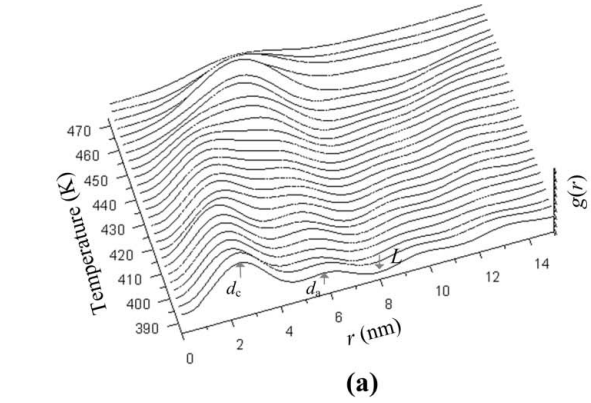

(a)

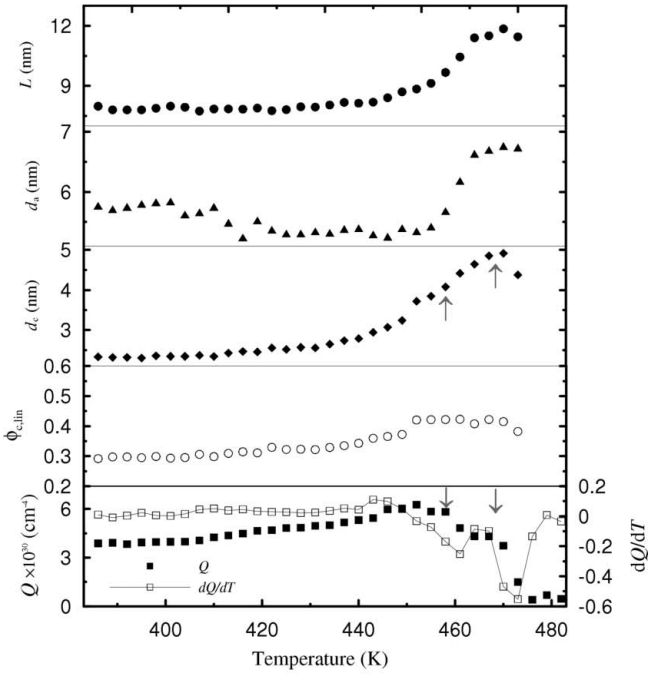

(b)

Figure 5
(*a*) Temperature scans of interface distribution function $g(r)$ recorded during the melting process (3 K min^{-1}) of PTN crystallized at T_c = 383 K. (*b*) Temperature dependence of the lamellar structures variables L, d_a, d_c, $\phi_{c,lin}$, Q and first derivative profile of Q (dQ/dT) during the heating process for PTN crystallized at 383 K. The arrows indicate two-step changes in structural parameters.

fully compensate the loss of crystallinity due to the melting of the α-crystal.

Fig. 3(*a*) shows the thermal evolution of the WAXS profiles recorded during melting of the PTN coexistent form after being crystallized at 423 K for 24 h. Computed from the WAXS/DSC data, the DSC thermogram, normalized crystallinity and intensity of emblematic Bragg peaks of the α- and β-crystals [marked by the arrows in Fig. 3(*a*)] at a melting process rate of 3 K min^{-1} are summarized in Fig. 3(*b*). Since the Bragg peaks of the α-crystals were seriously overlapped with those of the β-crystal for the PTN coexistent form, the total crystallinity could not objectively be separated into $W_{c,\alpha}$ and $W_{c,\beta}$. The total normalized crystallinity gradually decreases, *ca* 15%, with heating at $T_{m,1}$, due to the above-mentioned melting of the secondary α-crystal, and thereafter it continuously declines *ca* 25% on further heating to $T_{m,3}$. It is noteworthy that the Bragg diffraction intensities of the β-crystal (010_β and $1\bar{1}\bar{1}_\beta$) reduce more obviously than that of the α-crystal near $T_{m,3}$. We may sensibly attribute the melting peak of $T_{m,3}$ to the melting of the β-crystal. In Fig. 3(*b*), the intensities of 011_α and 012_α decrease remarkably at ~474 K, corresponding to the melting of the primary α-crystal ($T_{m,2}'$). However, the maximum intensities of 010_β and $1\bar{1}\bar{1}_\beta$ at ~478 K indicate that the $\alpha \rightarrow \beta$ phase transformation takes place and then the melting of the β-crystal, transformed from the α-crystal, gives rise in the $T_{m,2}''$.

3.3. Equilibrium melting temperature

To explore the structural stability of PTN polymorphism, we need to understand the difference between the equilibrium melting temperatures (T_m^0) of the α- and β-crystals. The Hoffman–Weeks equation (Hoffman *et al.*, 1976) is commonly utilized to determine T_m^0 by extrapolation of the experimental T_m, as $T_m = T_m^0(1-1/\gamma) + T_c/\gamma$, where $\gamma = l_c/l_c^*$ is the ratio of lamellar thickness l_c to the thickness l_c^* of the critical nucleus at T_c. To avoid the interference in thermal lag and recrystallization, the true melting temperature of the α-crystal ($T_{m,2}'$) can be estimated by temperature dependent on $W_{c,\alpha}$ [see examples in Figs. 2(*b*) and 3(*b*)] for a precise determination of the T_m^0 of the α-crystal. In the Hoffman–Weeks plot in Fig. 4, the two intersection points at 488 and 510 K, respectively, correspond to the T_m^0 of the PTN α- and β-crystals. The linear relation between $T_{m,3}$ and $T_{m,4}$ also confirms that $T_{m,3}$ arises from the melting of the primary β-crystal. $T^0_{m,\beta} > T^0_{m,\alpha}$ indicates that the β-crystal is a structurally stable phase, whereas the α-crystal is a metastable phase. Note that both values of the $T^0_{m,\beta}$ and $T^0_{m,\alpha}$ in our study are higher than the reported ($T^0_{m,\alpha}$ = 470 K and $T^0_{m,\beta}$ = 496 K) by Jeong *et al.* (2003). However, the $T^0_{m,\alpha}$ at 470 K for PTN may be an underestimate because we found that WAXS peaks of the α-crystal still exist above 470 K, as seen in Fig. 2(*a*).

3.4. The mechanism of PTN $\alpha \rightarrow \beta$ phase transformation

In semicrystalline polymer systems, an ideal lamellar structure of a crystalline–amorphous type can be characterized by the interface distribution function $g(r)$ (Ruland, 1977; Stribeck & Ruland, 1978). Fig. 5(*a*) shows interface distribution function profiles $g(r)$ computed from SAXS curves measured during melting (3 K min^{-1}) after isothermal crystallization at 383 K for 24 h. The $g(r)$ can be fitted by three Gaussian distributions to obtain the average values of lamellar thickness d_c, amorphous thickness d_a and long period L (Santa Cruz *et al.*, 1991). For the rigid main chains and non-filled lamellae stacks in the system, we relate the positions of the first maximum and secondary maximum to d_c and d_a, respectively. L is the first minimum position of $g(r)$ corresponding to $d_c + d_a$. The first maximum of $g(r)$

gradually laps over the secondary maximum with increasing temperature due to a broadening of the lamellar thickness distributions during the heating process.

Fig. 5(*b*) shows the changes in structural parameters of the lamellae stacks and invariant Q, during the melting of the PTN isothermal crystallized at 383 K for 24 h (3 K min^{-1}). Q is related to the morphological variables by $[Q = \int_0^\infty Iq^2 dq \propto \varphi_c(1-\varphi_c)\Delta\eta^2]$, where φ_c is the volume fraction of the crystalline phase and $\Delta\eta$ is the electron density difference between the crystalline and amorphous phases. The values of d_c, d_a and L vary little with temperature before the melting of secondary crystals ($T_{m,1}$). After $T_{m,1}$, d_c slightly increases and d_a slightly decreases, but L still varies little with the heating process between 413 and 433 K. This result suggests that the melting of the secondary α-crystal releases some amorphous chains to the noncrystalline zone, and then dynamic rearrangement of amorphous chains during the heating process, consequently shrinks the amorphous phases. With increasing temperature between 413 and 433 K in Fig. 5(*b*), the linear crystallinity $\phi_{c,lin}$ (= d_c/L) is increased, but the bulk crystallinity $W_{c,total}$ obtained by WAXS [see Fig. 2(*b*)] is almost constant. This difference in crystallinity between SAXS and WAXS is due to the fact that SAXS analysis relates only to the nanometer scale of lamellar stacks. We conjecture that this rearrangement contributes little to the bulk crystallinity, but it seems to be a preordering process for recrystallization at 433–443 K, as obtained by DSC and WAXS [see Fig. 2(*b*)].

Above 443 K, d_c, d_a and L rapidly increase with increasing temperature, but d_a increases relatively less than d_c. Other than the thermal expansion factor, the increase of d_c, d_a and L during the melting process can be attributed to the melting of polydisperse lamellar crystals (Ryan *et al.*, 1997). At the bottom of Fig. 5(*b*), the obvious rise of Q means that the term of $\varphi_c(1-\varphi_c)$ dominates Q during the heating process. When Q increases until the maximum, the volume fraction of crystals is close to 0.5. At further heating above 453 K, Q decreases rapidly until it vanishes, due to the crystals being completely melted. It is interesting to note that the changes in d_c and Q with increasing temperature from 443 to 473 K show a two-step behavior [as marked by the arrows in Fig. 5(*b*)]; furthermore the dQ/dT profile also reveals two transition peaks. These results of two-step changes in the structural parameters are consistent with endothermic peaks of $T_{m,2}'$ and $T_{m,2}''$ obtained by WAXS/DSC [Fig. 2(*b*)], corresponding to the melting of the primary α-crystals and remelting of the β-crystal transformed from the α-crystal. It is clear that d_c thickens during the $\alpha \rightarrow \beta$ transformation.

We found that the induction period or nucleation time of the β-crystal at T_c = 453 K is far longer than the time of the $\alpha \rightarrow \beta$ transformation that takes place during the heating process of 433–453 K at 3 K min^{-1}. We also found that the α-crystal can not completely transform into the β-crystal by the annealing process as long as the α-nuclei still exist. This may suggest that the β-nuclei attaches onto the surviving α-crystal to reduce the nucleation barrier for β-recrystallization during the melting process. If β-recrystallization forms *via* homogenous nucleation and/or develops new lamellae or lamellar stacks, the Bragg peak of 010_β should appear during the heating process as well as the coexistence α- and β-crystals. This is why the WAXS profile of the coexistence form was different from that of the $\alpha \rightarrow \beta$ transformation as seen in Figs. 1(*a*) and 2(*a*). These results indicate that the PTN $\alpha \rightarrow \beta$ transition is a typical melting–recrystallization process rather than the solid–solid phase transition which occurs in poly(butylene adipates) (Gan *et al.*, 2004).

4. Conclusion

The simultaneous WAXS/DSC measurement provides us with a suitable way to assign the multiple melting peaks with the primary and secondary crystals and phase transformation. $T_{m,1}$ was associated with the secondary crystals of the α-crystal and both $T_{m,3}$ and $T_{m,4}$ arose from the melting of the β-crystal. The broad peak of $T_{m,2}$ could be separated into $T_{m,2}'$ and $T_{m,2}''$, which were attributed to the melting of the primary lamellae of the α-crystal and the remelting of the β-crystal transformed from the α-crystal, respectively. The correct assignation of multiple melting peaks enabled us to extrapolate precisely the equilibrium melting temperature T_m^0. Both equilibrium melting temperatures of α- and β-crystals ($T_{m,\alpha}^0$ and $T_{m,\beta}^0$) are 488 and 510 K, respectively. Taking into account all the results presented above, we attribute PTN $\alpha \rightarrow \beta$ transformation to the surface melting of α-lamellae and then surface recrystallization of the β-crystal. For the melting–recrystallization, the α-lamellae do not monotone melt at once; whereas the partial α-lamellae start to melt at lamellae boundaries. Subsequently, the melting chains near surviving lamellar surfaces activate and alter their conformation to form stems of β-crystal on the diminishing α-crystal surface.

The authors thank Dr H. Chauh of the Shell Chemical Company for his kind supply of poly(trimethylene 2,6-naphthalate) samples.

References

Blundell, D. J. (1987). *Polymer*, **28**, 2248–2251.
Blundell, D. J. & Osborn, B. N. (1983). *Polymer*, **24**, 953–958.
Cheng, S. Z. D., Cao, M. Y. & Wunderlich, B. (1986). *Macromolecules*, **19**, 1868–1876.
Chuang, W. T., Yeh, W. J. & Hong, P. D. (2002). *J. Appl. Polym. Sci.* **83**, 2426–2433.
Gan, Z., Kuwabara, K., Abe, H., Iwata, T. & Doi, Y. (2004). *Biomacromolecules*, **5**, 371–378.
Ghosh, A. K., Woo, E. M., Sun, Y. S., Lee, L. T. & Wu, M. C. (2005). *Macromolecules*, **38**, 4780–4790.
Ho, R. M., Lin, C. P., Tsai, H. Y. & Woo, E. M. (2000). *Macromolecules*, **33**, 6517–6526.
Hoffman, J. D., Davis, G. T. & Lauritzen, J. I. Jr (1976). *Treatise on Solid State Chemistry*, Vol. 3, edited by N. B. Hannay. New York: Plenum Press.
Hong, P. D., Chuang, W. T. & Hsu, C. F. (2002). *Polymer*, **43**, 3335–3343.
Hsiao, B. S., Gardner, K. H. Wu, D. Q. & Chu, B. (1993*a*). *Polymer*, **34**, 3996–4003.
Hsiao, B. S., Gardner, K. H., Wu, D. Q. & Chu, B. (1993*b*). *Polymer*, **34**, 3986–3995.
Jeong, Y. G., Jo, W. H. & Lee, S. C. (2003). *Polymer*, **44**, 3259–3267.
Jeong, Y. G., Jo, W. H. & Lee, S. C. (2004). *Polymer*, **45**, 379–384.
Lai, Y. J., Sun, Y. S., Jeng, U., Lin, J. M., Lin, T. L., Sheu, H. S., Chuang, W. T., Huang, Y. S., Hsu, C. H., Lee, M. T., Lee, H. Y., Liang, K. S., Gabriel, A. & Koch, M. H. J. (2006). *J. Appl. Cryst.* **39**, 871–877.
Ruland, W. (1977). *Colloid Polym. Sci.* **255**, 417–427.
Ryan, A. J., Stanford, J. L., Bras, W. & Nye, T. M. W. (1997). *Polymer*, **38**, 759–768.
Santa Cruz, C., Stribeck, N., Zachmann, H. G. & Baltá Calleja, F. J. (1991). *Macromolecules*, **24**, 5980–5990.
Stribeck, N. & Ruland, W. (1978). *J. Appl. Cryst.* **11**, 535–539.
Sun, Y. S. & Woo, E. M. (1999). *Macromolecules*, **32**, 7836–7844.
Velikov, V. & Marand, H. (1993). *Polym. Prepr.* **34**, 835–837.